Magnetic and Electric Responsive Hydrogel–Magnetic Nanocomposites for Drug-Delivery Application

N. Narayana Reddy,[1] Y. Murali Mohan,[1]* K. Varaprasad,[1] S. Ravindra,[1] P. A. Joy,[2] K. Mohana Raju[1]

[1]*Synthetic Polymer Laboratory, Department of Polymer Science and Technology, Sri Krishnadevaraya University, Anantapur 515003, Andhra Pradesh, India*
[2]*Physical and Materials Chemistry Division, National Chemical Laboratory, Pune 411008, India*

Received 28 July 2010; accepted 25 December 2010
DOI 10.1002/app.34016
Published online 23 May 2011 in Wiley Online Library (wileyonlinelibrary.com).

ABSTRACT: Magnetic and electrically responsive hydrogel networks were developed for drug-delivery applications. The hydrogel matrices were synthesized by the polymerization of acrylamide monomer in the presence of carboxymethylcellulose (CMC) or methylcellulose (MC) with *N*,*N*-methylenebisacrylamide, a crosslinker with the redox initiating system ammonium persulfate/tetramethylethylenediamine. The magnetic nanoparticles were generated throughout these hydrogel matrices by an *in situ* method by the incorporation of iron ions and their subsequent reduction with ammonia. A series of hydrogel–magnetic nanocomposites (HGMNCs) were developed with various CMC and MC compositions. The synthesized HGMNCs were characterized with spectral (Fourier transform infrared and ultraviolet–visible spectroscopy), X-ray diffraction, thermal, and microscopy methods. These HGMNCs contained iron oxide (Fe_3O_4) nanoparticles with an average particle size of about 22 nm, as observed by transmission electron microscopy. The dielectrical properties of the pure hydrogel (HG); the hydrogel loaded with iron ions, or the hydrogel iron-ion composite (HGIC); and the HGMNCs were measured. These results suggest that HGMNCs exhibited higher dielectric constants compared to HG and HGICs. The curcumin loading and release characteristics were also measured for HG, HGIC, and HGMNC systems. These data revealed that there was a sustained release of curcumin from HGMNCs because of the presence of magnetic nanoparticles in the hydrogel networks. © 2011 Wiley Periodicals, Inc. J Appl Polym Sci 122: 1364–1375, 2011

Key words: hydrogels; magnetic polymers; nanocomposites; nanoparticle; nanotechnology

INTRODUCTION

Polysaccharide-based hydrogels are a class of biomaterials widely used in medicine, pharmacy, and biology.[1] These hydrogels have been widely employed in the development of controlled release formulations of pharmaceutical drugs.[2,3] Polysaccharide-based hydrogels have also been employed for the removal of heavy metals and dyes from wastewater (water purification)[4,5] and for separation membrane applications.[6,7]

Hydrogel–magnetic nanocomposites (HGMNCs) prepared by the employment of polysaccharide and magnetic nanoparticles [iron oxide (Fe_3O_4) or maghemite (γ-Fe_2O_3)] have been shown to have sensitivity to an external stimulus, that is, to an applied magnetic field.[8,9] Many researchers have studied such hydrogels, aiming for the controlled release of drugs for targeting cancer cells,[10] the separation of biomolecules,[11] the immobilization of enzymes,[12] and hyperthermia applications.[13] Hydrogel-embedded magnetic nanoparticles have been employed as magnetically modulated drug-delivery systems with the feasibility of delivering drugs at controlled rates.[14–16] The release of drugs from such drug-delivery systems is dependent on magnetic field characteristics and polymer/hydrogel properties.[17]

Materials having a wide range of magnetodielectric properties have been developed with a view to use them for advanced applications in communication and miniaturization.[18–20] The hybrid materials consisting of polymers/hydrogels and magnetite and possessing magnetic and electrical properties have developed for recording media,[21] inductive/capacitive purposes, and medical applications.[22] The dielectrical properties and the formation of magnetic nanoparticles for subsequent drug-delivery applications depend on the presence of the free OH groups in cellulose. Therefore, two cellulose derivatives, namely, carboxymethylcellulose (CMC) and methylcellulose

**Present address:* Cancer Biology Research Center, Sanford Research/University of South Dakota, Sioux Falls, SD 57105.

Correspondence to: K. M. Raju (krmohan@yahoo.com).

Contract grant sponsor: (to K.M.R. and N.N.R.): University Grants Commission (UGC), Government of India, New Delhi; contract grant number: UGC Sanction Letter No. F. 37-339/2009.

(MC), were used in this investigation to develop novel HGMNCs having enhanced dielectrical properties. Furthermore, the presence of cellulose in the hydrogel network enhances water absorbency,[23] which is responsible for the formation of more Fe_3O_4 in the HGMNCs. The developed nanocomposites showed enhanced dielectric properties when compared to simple hydrogels. These biocompatible HGMNCs showed sustained drug-release characteristics.

EXPERIMENTAL

Materials

Acrylamide (AM), *N,N′*-methylenebisacrylamide (MBA), *N,N,N′,N″*-tetramethylethylenediamine (TMEDA), and ammonium persulfate (APS) were purchased from Aldrich Chemical Co., Inc. (Milwaukee, WI). MC, CMC, ferrous chloride tetrahydrate ($FeCl_2{\cdot}4H_2O$), and ferric trichloride hexahydrate ($FeCl_3{\cdot}6H_2O$) were purchased from Merck (Mumbai, India). Ammonia solution in water (28%) was obtained from S. D. Fine Chemicals, Ltd. (Mumbai, India). Curcumin, a naturally occurring drug, was a gift sample from Natural Remedies Private, Ltd. (Bangalore, India). All of the chemicals and reagents were used without further purification. Double-distilled water was used for the preparation of all solutions in this study.

Preparation of the hydrogels

Polyacrylamide (PAM)/MC and PAM/CMC hydrogels were synthesized with free-radical polymerization with MBA as a crosslinker and APS/TMEDA as redox-initiating pair according to a procedure reported earlier.[24] In a typical polymerization reaction, 1 g of AM and different amounts of CMC/MC (0.1, 0.2, 0.3, and 0.4 g) were dissolved in 4 mL of distilled water with stirring for 10 min in a 50-mL beaker. To this, 1 mL of MBA (1 g in 100 mL), 1 mL of TMEDA (1 g in 100 mL), and 1 mL of APS (5 g in 100 mL) solutions were sequentially added. After the addition of these reactants, the temperature of the system was raised to 50°C for 15 min. After the completion of gel formation, the hydrogel was immersed in distilled water at room temperature for 24 h to remove the unreacted materials present in the hydrogel network. The prepared hydrogels were dried in a vacuum oven at 60°C for 3 h and then dried at room temperature for 24 h.

Preparation of the HGMNCs

For this, a dry PAM–MC or PAM–CMC hydrogel sample (500 mg) was placed in a 500-mL beaker containing 100 mL of double-distilled water and allowed to swell completely for 24 h. The swollen hydrogel was then transferred to another beaker containing 200 mL of an aqueous solution of 2.1 g of iron(II) chloride tetrahydrate and 5.8 g of iron(III) chloride hexahydrate (molar ratio of 1 : 2) and equilibrated for 24 h. The hydrogel loaded with iron(II) and iron(III), or hydrogel iron-ion composite (HGIC) was removed from the iron salt mixed solution, superficially washed with double-distilled water, placed in a 50 mL of a 0.5*M* ammonia solution (28 wt %), and left overnight. During this process, most of the iron ions in the hydrogel networks converted into ferrite nanoparticles or magnetic nanoparticles. The resultant black hybrid hydrogel, that is, HGMNC was removed, washed with double-distilled water, and allowed to dry in oven at 60°C.

Swelling studies

Dried hydrogels ($\sim$ 10 mg) were equilibrated in distilled water at 30°C for 3 days. The equilibrium swelling capacity or swelling ratio (Q) of the gels was calculated with the equation $Q = W_e/W_d$, where W_e is the weight of the swollen hydrogel at equilibrium and W_d is the dry weight of the pure hydrogel.

Characterization

Fourier transform infrared (FTIR) spectroscopy

FTIR spectroscopy was performed for the pure hydrogel (HG), HGIC, and HGMNC with an MB3000 model spectrophotometer (ABB Co., Quebec, Canada).

Thermogravimetric analysis (TGA)

The thermal analyses of HG, HGIC, and HGMNC were evaluated on a SDT Q 600 TGA instrument (TA Instruments-Water LLC, Newcastle, DE) at a heating rate of 10°C/min under a constant nitrogen flow (100 mL/min). The samples were run from 40 to 800°C.

Differential scanning calorimetry

Differential scanning calorimetry of HG, HGIC, and HGMNC were studied with a SDT Q 600 DSC instrument (TA Instruments-Water LLC) at a heating ramp of 10°C/min under a constant nitrogen flow (100 mL/min). The samples were run from 40 to 400°C.

Scanning electron microscopy (SEM)

The surface morphology of HG, HGIC, and HGMNC were studied with a JEOL JSM 840A scanning electron microscope (Tokyo, Japan) at an accelerating voltage of 15 kV. All of the samples

were dried *in vacuo* at room temperature and coated with gold before scanning.

Transmission electron microscopy (TEM)

The size of the magnetic nanoparticles in gel network was determined with a Technai F12 transmission electron microscope (Tokyo, Japan). For this study, we prepared the samples by placing a drop of an aqueous solution of HGMNC on a carbon-coated copper grid and subsequently drying them in air before transferring them to the microscope, which was operated at an accelerated voltage of 120 kV.

X-ray diffraction (XRD)

The XRD studies of HG, HGIC, and HGMNC were carried out on a Rikagu diffractometer (Rikagu, Tokyo, Japan) employing rotting anode mode Ru-H3R (Cu radiation) running at 40 kV and 40 mA.

Magnetization measurements

The magnetization and hysteresis loop were measured at room temperature with a vibrating sample magnetometer (model 7300 VSM system, Lake Shore Cryotronic, Inc., Westerville, OH).

Dielectric properties

The dielectric measurements were carried out in the frequency range 10 Hz to 1 MHz with an LCR (Inductance, Capacitance, Resistance) meter bridge (HIOKI 3532-50, Tokyo, Japan), and the dielectric constant (ε') was calculated with the following relation:

$$\eta' = 14.37 C_p d / A \eta_o \quad (1)$$

where d is the thickness of the hydrogel sample, A is the cross-sectional area of the hydrogel sample, C_p is the capacity in picofarads (pF), and ε_o is the permittivity of free space.

Drug loading

Curcumin is a principal curcuminoid in turmeric that is derived from the rhizomes of *Curcuma longa*. This naturally occurring yellow polyphenolic compound is widely used in traditional Ayurvedic and Chinese medicine. Curcumin exhibits wide range of pharmacological applications, such as anti-inflammation, anti-human immunodeficiency virus, antimicrobial, antioxidant, antiparasitic, antimutagenic, and anticancer applications,[25–29] with almost no intrinsic toxicity to normal cells. Therefore, this compound was chosen to load into hydrogels for drug-delivery applications. The curcumin drug was loaded in the hydrogel samples by immersion of the hydrogel in the drug solution. For this experiment, a 50-mg hydrogel sample was taken and immersed in 20 mL of drug solution (5 mg/20 mL, 4 : 6 acetone:distilled water). The amount of drug included in the hydrogel sample was determined by ultraviolet–visible spectroscopy. To determine the maximum absorbance of curcumin, the ultraviolet–visible spectra for the pure curcumin solution was taken, and the maximum absorbance was found at 472.2 nm. The percentage of drug loading and encapsulation efficiency were calculated with the following equations:

$$\% \text{ Encapsulation efficiency} = [\% \text{ actual loading} / \% \text{ theoretical loading}] \times 100 \quad (2)$$

$$(\% \text{ of theoretical loading} = \text{amount of drug added} / \text{amount of polymer} \times 100) \quad (3)$$

Release of curcumin

The *in vitro* release studies of the curcumin drug were carried out by placement of the dried and curcumin loaded hydrogels in definite volumes, that is, 50 mL (20 mL of water and 30 mL of acetone) of releasing medium [pH 7.4 phosphate buffer (PBS) prepared with a 2 : 3 water:acetone mixture], and the dissolution medium was placed on a rotary shaker (Remi Instruments Limited, model CIS-24BL, Vasai, India) at 100 rpm at 37°C. The amount of drug release from the hydrogel to the medium was determined by the withdrawal of 3 mL of aliquots of the solution at selected specific time intervals. The volume withdrawn was immediately replaced with an equal volume of PBS. The amount of drug release was measured specrophotometrically. The absorption of the solutions of curcumin drug was measured at λ_{max} at 472.2 nm

The percentage cumulative release (R) of curcumin from the hydrogel was calculated with the following equation:

$$R = M_t / M_o \times 100 \quad (4)$$

where M_t is the amount of drug released at time t and M_o is the initial loaded drug amount.

RESULTS AND DISCUSSION

HGMNC formation

Because of the existence of anionic carboxymethyl and methyl groups in the CMC/MC polymer chains in hydrogels, the iron(II) and iron(III) cations could easily bind to the hydrogel networks from the

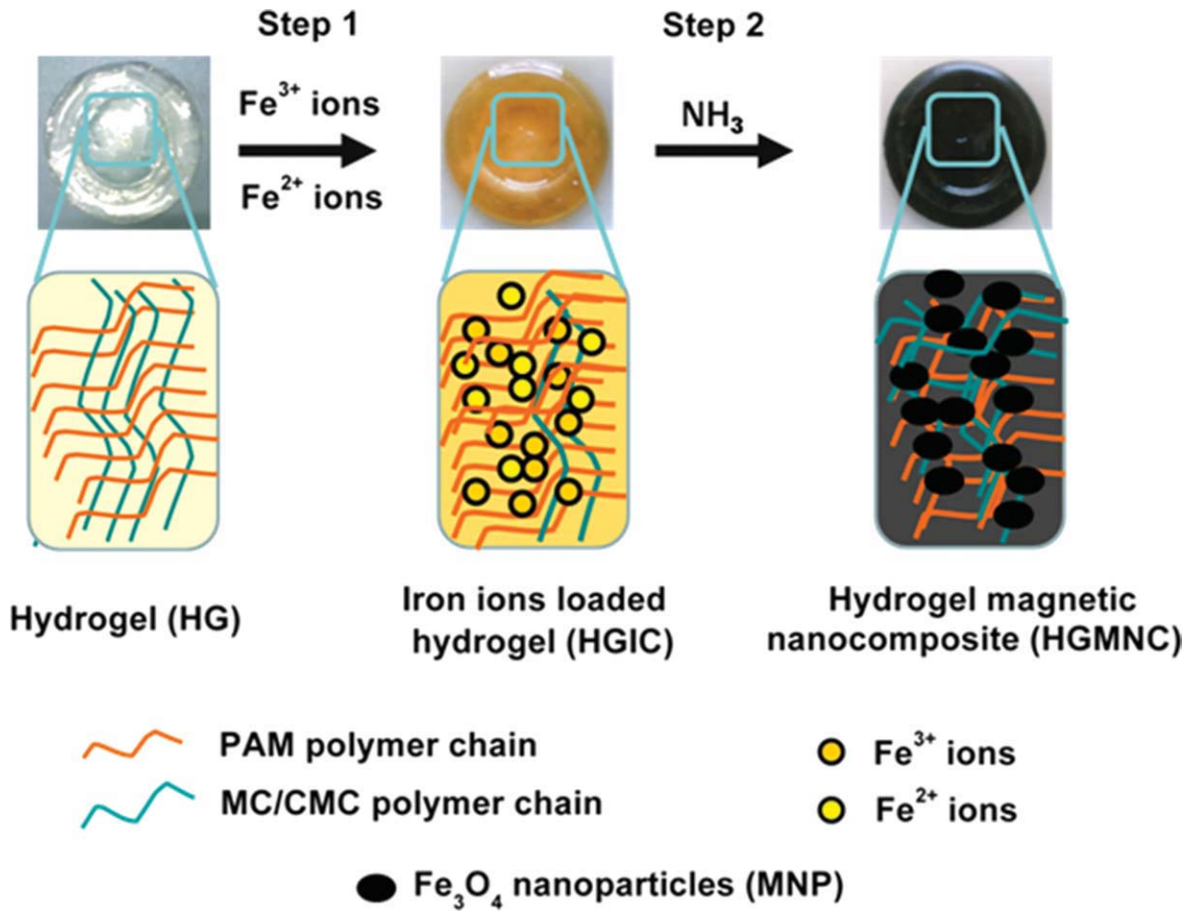

Figure 1 Schematic representation of the HGMNC preparative route. The transparent hydrogel (left) represents pure PAM–CMC or PAM–MC hydrogels obtained from the free-radical crosslinking polymerization from AAM/CMC or AAM/MC in the presence of MBA and APS/TMEDA. The yellow hydrogel (center) indicates HGIC. The black hydrogel (right) indicates HGMNC. [Color figure can be viewed in the online issue, which is available at wileyonlinelibrary.com.]

aqueous mixed solutions of iron(II) chloride tetrahydrate and iron(III) chloride hexahydrate via electrostatic interactions. These hydrogel networks acted as templates for the *in situ* deposition of magnetic Fe_3O_4 particles by the following reduction reaction induced by ammonia:

$$Fe^{+2} + 2Fe^{+3} + 8OH^- \rightarrow Fe_3O_4 \downarrow + H_2O \qquad (5)$$

Figure 1 gives a schematic illustration of the formation process of HGMNC. The corresponding hydrogels were also embedded to visualize the original color of the hydrogels during the preparation steps. The loading of iron ions into the hydrogel could be followed visually by observation of the color change of the hydrogel from transparent to yellow–orange (step 1, HG to HGIC). The color intensity was a function of the initial iron-ion concentration of the solution and was retained after washing with water; this suggested a strong binding ability of this hydrogel to iron ions. When ammonia was added, a rapid color change of the swollen hydrogel from yellow–orange to black was observed (step 2, HGIC to HGMNC). This indicated that the reduction reaction could have occurred spontaneously and resulted in the formation of the Fe_3O_4 nanoparticles in the hydrogel networks.

The swelling capacities of the PAM–CMC and PAM–MC hydrogels composed of different amounts (100–400 mg) of CMC and MC are shown in Figure 2(A,B), respectively. The increase of cellulose polymer content in the hydrogel network increased the swelling capacity of the hydrogels. This was due to the entrapment of more hydrophilic polymeric chains (CMC or MC) in the hydrogel networks, which assisted in improving the swelling characteristic of the gel systems. At all the compositions, the PAM–CMC hydrogels exhibited higher swelling ratios than PAM–MC hydrogels. An improved absorption capacity in the PAM–CMC hydrogels was observed because of the presence of more hydrophilic chains containing hydrational functional groups on the polymeric chains, such as –OH and $^-OCH_2COO^-Na^+$.[30] After treating the hydrogels

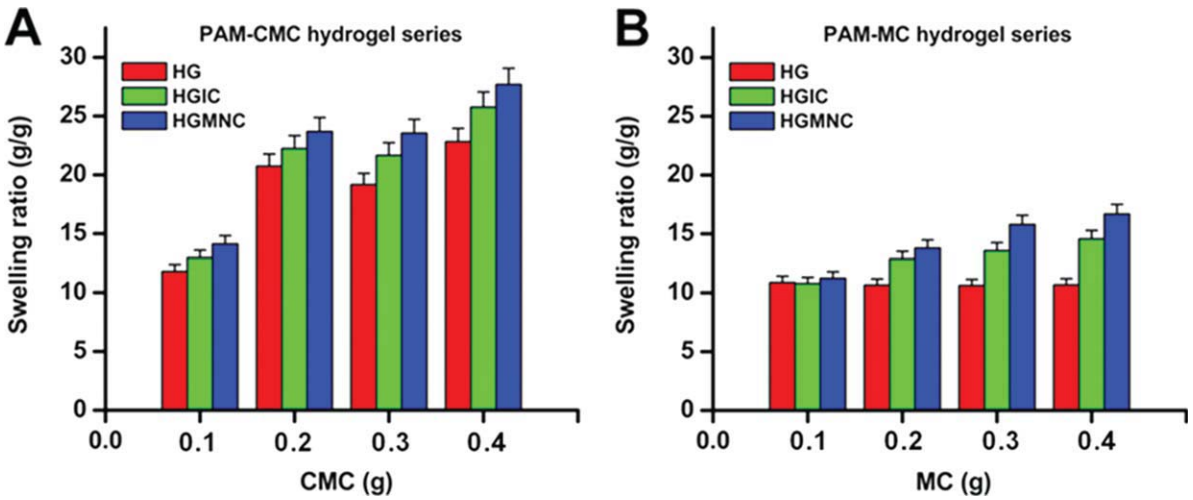

Figure 2 Swelling behavior of PAM–CMC, PAM–MC HGs, HGICs, and HGMNCs. [Color figure can be viewed in the online issue, which is available at wileyonlinelibrary.com.]

with ferrous/ferric ions (HGIC), the repulsive forces between the hydrogel network chains increased; this ultimately led to the improved swelling behavior of HGICs compared to HGs. This phenomenon was quite uniform for all of the HGIC hydrogel systems, as found in our previous hydrogel silver nanoparticle studies.[31] A further increase in the swelling capacity was observed after the addition of the reducing agent [NH_3] to HGIC, which gave HGMNC. This pattern of swelling was reasonable for HGMNCs because once the magnetic nanoparticles were formed inside the gel networks, the overall porosity of the system increased; this allowed for a greater number of water molecules inside the gel.[32] The order of swelling capacity of the various gel systems was as follows: HGMNC > HGIC > HG (Fig. 2). PAM hydrogels with higher CMC and MC contents (CMC/MC = 0.4 g) and its iron ion/magnetic nanoparticles had higher swelling capacities in the PAM–CMC/MC series gels. Therefore, these hydrogel samples were used for further characterization and dielectrical and drug-delivery studies.

Characterization of HGMNCs

FTIR spectroscopy

The formation of magnetic nanoparticles in the hydrogel networks was confirmed by FTIR spectroscopy and XRD studies. The FTIR spectra of the PAM–CMC/PAM–MC hydrogels and their nanocomposites are presented in Figure 3. In all the hydrogels (PAM–CMC and PAM–MC hydrogels series), some common peaks were observed at 3430 cm^{-1} (A), 3160 cm^{-1} (B), 1664 cm^{-1} (C), and 1460 cm^{-1} (D); these peaks were due to groups corresponding amide, hydroxyl/ester stretching vibrations of PAM, and CMC and MC chains.[19] The C-O-C corresponding stretching peaks of CMC/MC were observed at 1120 cm^{-1} (E). However, an additional peak at 583 cm^{-1} (F) was observed in the case of HGMNCs (because of the presence of Fe_3O_4 nanoparticles). This is the common stretching peak obtained due to Fe-O vibrations of Fe_3O_4 nanoparticles. Therefore, the IR spectra confirmed the presence of Fe_3O_4 nanoparticles in the hydrogel networks.

XRD

The XRD patterns for the HGMNCs are shown in Figure 4. The HGs (PAM–CMC and PAM–MC hydrogels) showed a common broad diffraction peak (2θ) at 20°, which was due to the amorphous nature of PAM and the carbohydrate polymers. This is a known characteristic of hydrogels.[33] A similar

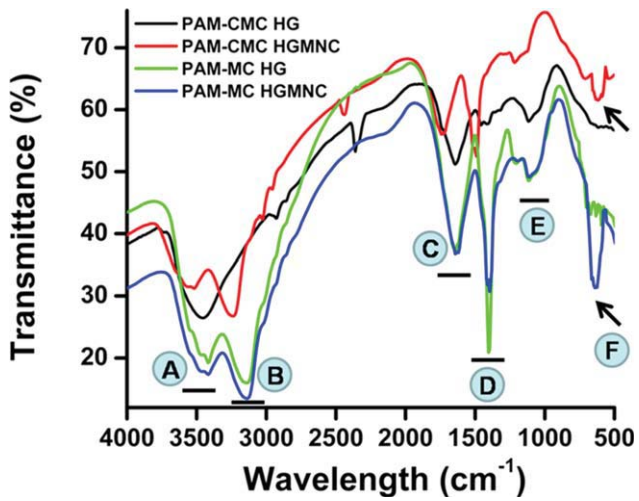

Figure 3 FTIR spectra of PAM–CMC, PAM–MC HGs, and HGMNCs. [Color figure can be viewed in the online issue, which is available at wileyonlinelibrary.com.]

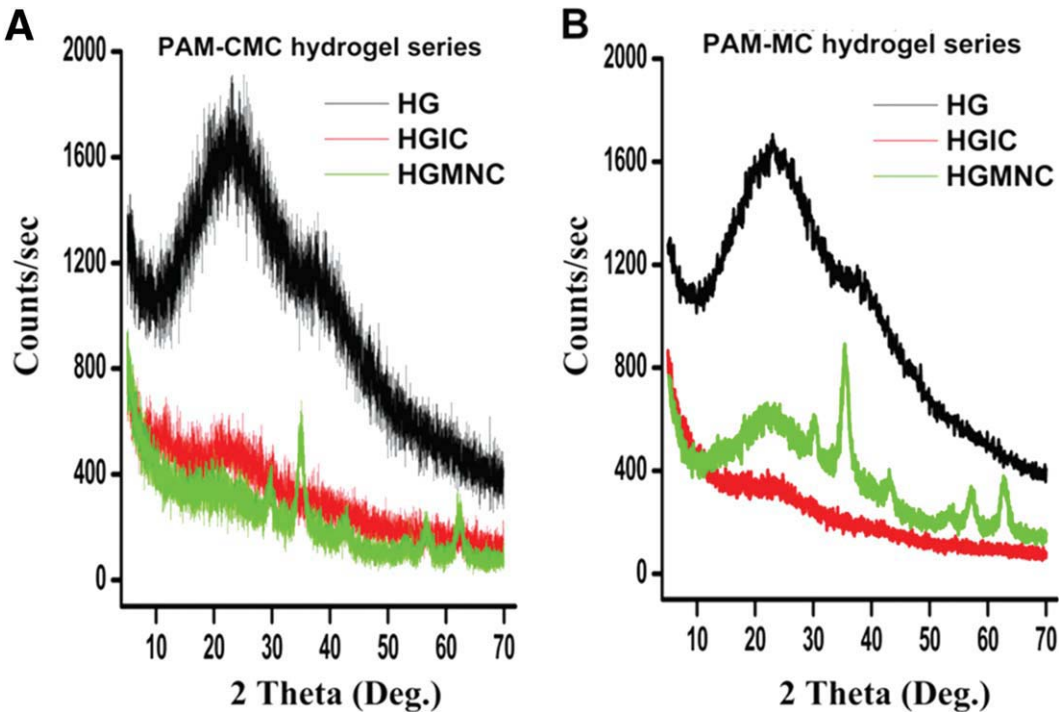

Figure 4 XRD patterns of PAM–CMC, PAM–MC HGs, HGICs, and HGMNCs. [Color figure can be viewed in the online issue, which is available at wileyonlinelibrary.com.]

phenomenon (no crystalline peaks) was observed in the case of the HGICs. However, the characteristic peaks of Fe_3O_4 nanoparticles were observed at 2θ = 30.1, 35.5, 43.1, 57, and 62.6° for both HGMNCs. These peaks were consistent with the peaks reported by Huang et al.[34] for pure Fe_3O_4 nanoparticles with a spherical structure. Therefore, the results confirmed that Fe_3O_4 nanoparticles were incorporated into the PAM–CMC and PAM–MC hydrogel networks. Furthermore, the hybridization process showed no phase change of the magnetic Fe_3O_4 nanoparticles; thereby, they maintained the magnetic functions.

TGA

The TGA of the hydrogels is depicted in Figure 5. In all cases, thermal degradation curves showed three weight loss stages. In both the PAM–CMC and PAM–MC hydrogel series, it was found that the initial degradation temperature (step 1, weight loss) of HGs was higher than that of the HGIC and HGMNC. This observation was due to the catalytic property of the Fe_3O_4 nanoparticles.[35] At 800°C, the PAM–CMC and PAM–MC HGs were completely degraded (100% weight loss), and no weight remained. In the case of HGICs, because of the presence of iron ions, 8.4% (HGIC of the PAM–CMC hydrogel) and 3.2% (HGIC of the PAM–MC hydrogel) of residue remained after 800°C. This residue was greater in the case of the HGMNCs. It was noticed that 14.5 and 9.7% residue remained for the PAM–CMC and PAM–MC based magnetic nanocomposites, respectively, at 800°C. The residue at 800°C for HGMNCs indicated the percentage of Fe_3O_4 formed in the gel network. A higher percentage of Fe_3O_4 was formed for the PAM–CMC gels. This was due to the reason that the PAM–CMC hydrogels absorbed a higher amount of water, which led to the absorbance of more iron ions and, thereby, the formation of a greater amount of Fe_3O_4.

DSC

Figure 6 illustrates the DSC curves of HG, HGIC, and HGMNC of the PAM–CMC and PAM–MC hydrogels. For each hydrogel sample investigated, there was an abrupt change in the heating curve with the presence of iron ions (HGIC) or Fe_3O_4 nanoparticles (HGMNC) in the hydrogel networks.

The endothermic peaks of the HG, HGIC, and HGMNCs between 269 and 300°C resulted in the melting process of the gel networks. This behavior depended on the hydrogel crosslinked networks. The melting peak temperatures were higher for HG [300.5°C in Fig. 6(A) and 285.4°C in Fig. 6(B)] compared to HGIC [272.4°C in Fig. 6(A) and 269.7°C in Fig. 6(B)] and HGMNC [278.2°C in Fig. 6(A) and 269.5°C in Fig. 6(B)]. Similar to the TGA experiments, the DSC curves also suggested that the initial decomposition was higher in the case of HGIC and HGMNC compared to HG.

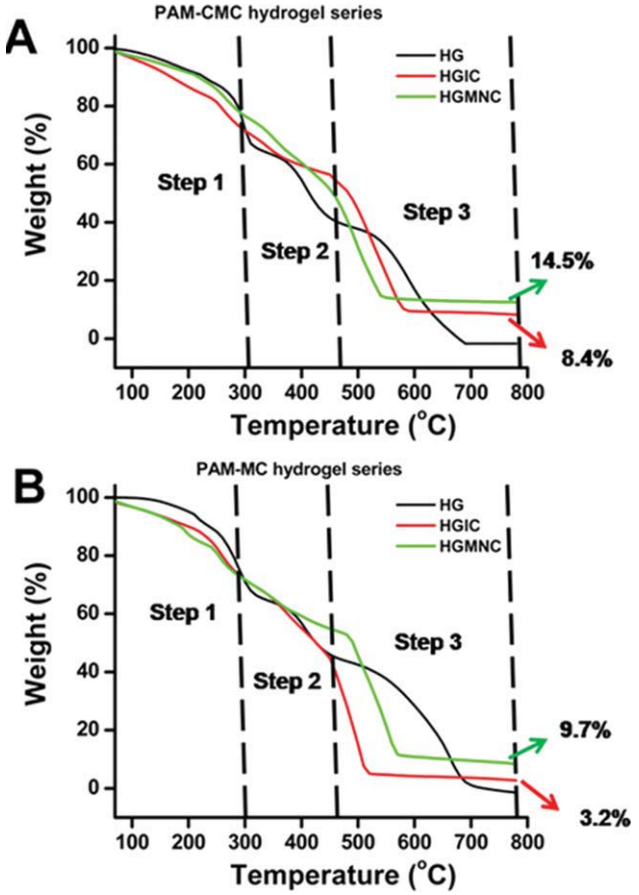

Figure 5 Thermogravimetric curves of PAM–CMC, PAM–MC HGs, HGICs, and HGMNCs. [Color figure can be viewed in the online issue, which is available at wileyonlinelibrary.com.]

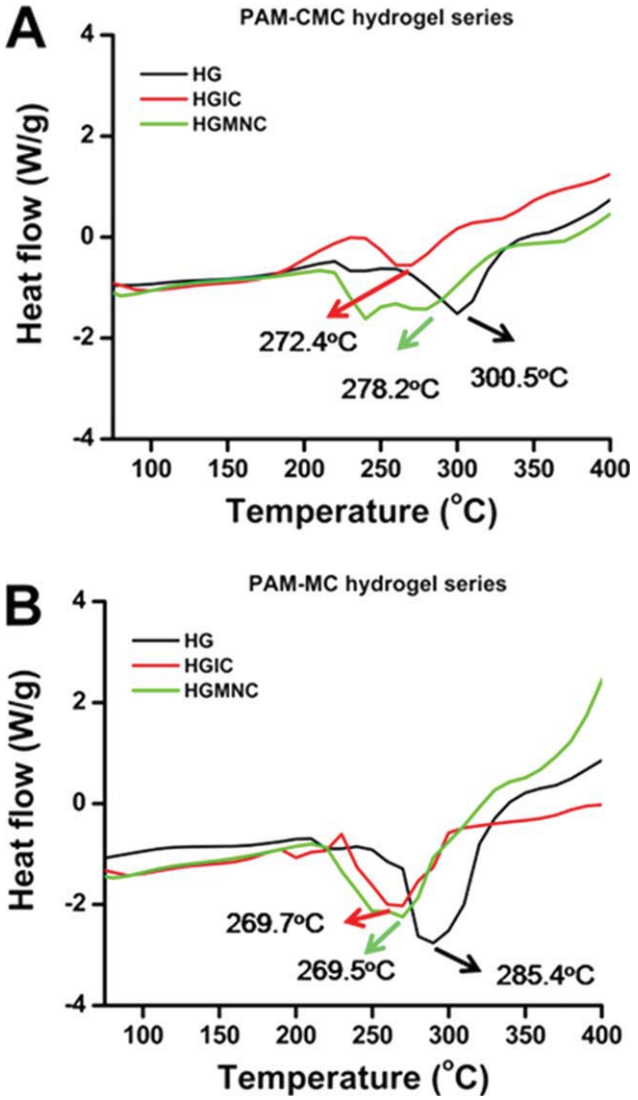

Figure 6 Differential scanning micrographs of PAM–CMC, PAM–MC HGs, HGICs, and HGMNCs. [Color figure can be viewed in the online issue, which is available at wileyonlinelibrary.com.]

Microscopic studies

SEM

Electron microscopy is usually used to distinguish morphological changes in a sample. In this study, SEM was used to visualize the changes in the hydrogel networks after iron-ion networks were loaded into the hydrogel and after the formation of Fe_3O_4 magnetic nanoparticles in their networks. The morphology of HG, HGIC, and HGMNC of the PAM–CMC and PAM–MC hydrogels are presented in Figure 7. The SEM micrograph images of the HGs [Fig. 7(A,B), HG] indicated a uniform surface, whereas HGIC showed randomly aggregated structures (clusters, shown with black arrows) throughout the gel surface [Fig. 7(A,B), HGIC]. However, in the case of the HGMNCs, a clear formation of nanostructures were found (yellow/light arrows) all over the hydrogel [Fig. 7(A,B), HGMNC]. However, these were only aggregated bulk Fe_3O_4 nanoparticles, whereas the formation of individual nanoparticles could be clearly seen in magnified SEM images of the HGMNCs (Fig. 8).

TEM

The exact size of the Fe_3O_4 nanoparticles generated in the PAM–CMC and PAM–MC hydrogel networks were characterized by TEM. The TEM images of the Fe_3O_4 nanoparticles extracted from the HGMNCs are shown in Figure 9. These images clearly revealed an average Fe_3O_4 nanoparticle grain size of 22.45 nm for HGMNC of PAM–CMC [Fig. 9(A)] and 23.6 nm for HGMNC of PAM–MC [Fig. 9(B)]. The observations revealed uniform particle formation instead of the formation of large clusters.

Magnetic properties

It is well known that nanosized Fe_3O_4 particles exhibit superparamagnetic properties. According to

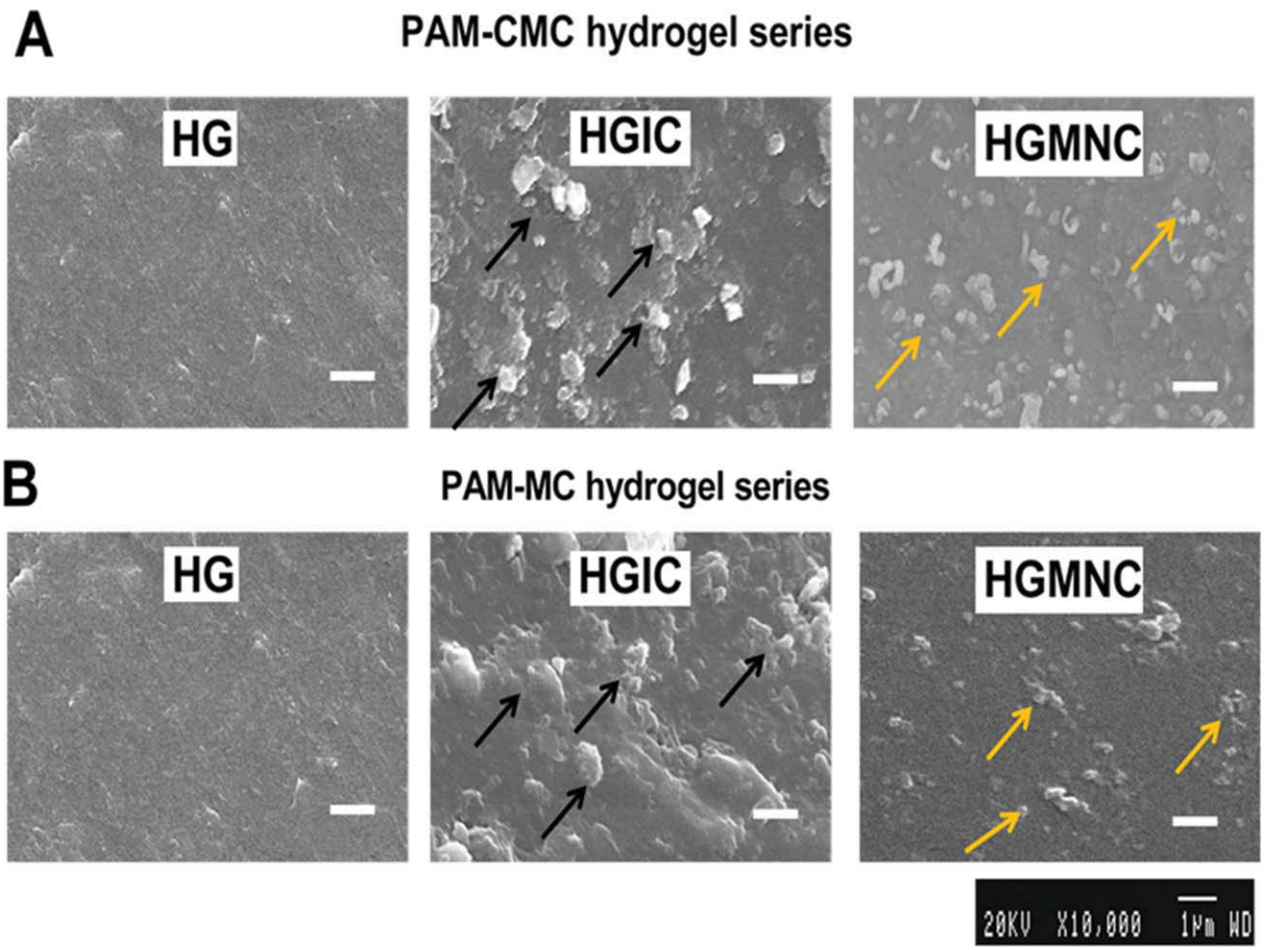

Figure 7 SEM images of PAM–CMC, PAM–MC HGs, HGICs, and HGMNCs. [Color figure can be viewed in the online issue, which is available at wileyonlinelibrary.com.]

TEM analysis, the developed Fe_3O_4 nanocomposites may have also shown superparamagnetic properties, which could be estimated by the measurement of their magnetic saturation with a magnetometer (VSM). Figure 10 illustrates the magnetization loops [magnetization vs applied field] of HGMNCs.

The variation in the magnetic moments of the prepared HGMNCs was investigated as a function of the variation of the magnetic field in the range of −15,000 to 15,000 Oe. The saturation magnetization (M_s) and coercivity of the PAM–CMC HGMNC were found to be 8.9 emu/g and 14,731 Oe. In the case of

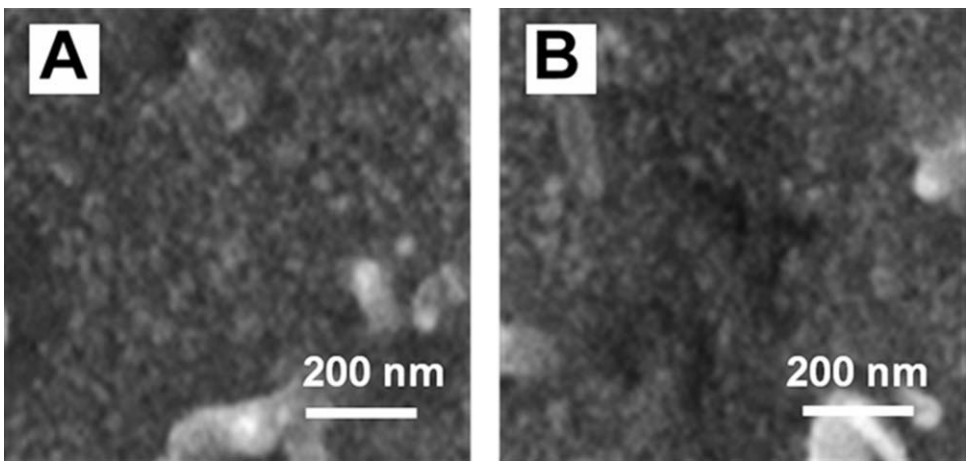

Figure 8 SEM images of (A) PAM–CMC HGMNCs and (B) PAM–MC HGMNCs.

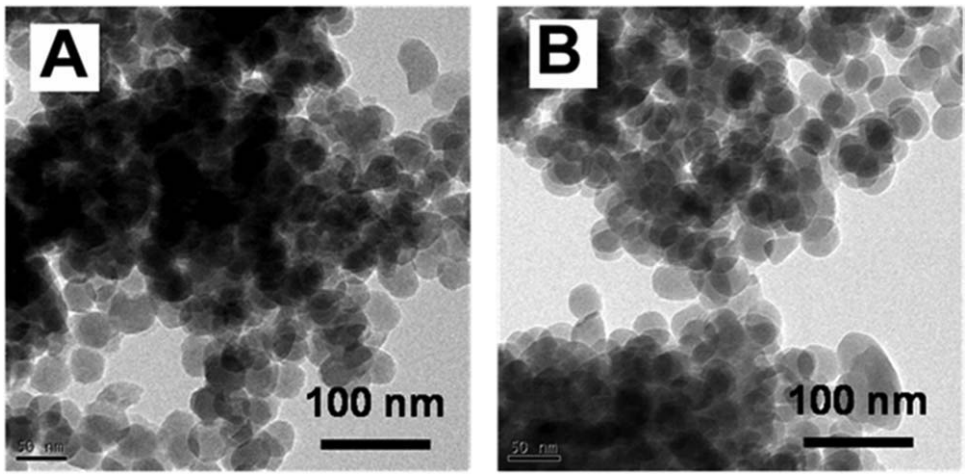

Figure 9 TEM images of the magnetic nanoparticles extracted from (A) PAM–CMC HGMNCs and (B) PAM–MC HGMNCs.

PAM–MC HGMNC, the M_s value was 6.4 emu/g, and the coercivity was 12,345 Oe. This variation could be expected because a smaller amount of Fe_3O_4 nanoparticles was present in HGMNC of PAM–MC compared to HGMNC of PAM–CMC (from TGA study, Fig. 5). Further, these M_s values of these composites (8.9 and 6.4 emu/g) were far below those of pure magnetic nanoparticles (Fe_3O_4, 66.1 emu/g). These low values were anticipated because of the presence of about 14.5% (PAM–CMC HGMNC) or 9.7% (PAM–MC HGMNC) magnetic nanoparticles only in the hydrogels. The theoretical M_s value of PAM–CMC HGMNC was calculated as follows: $M_s = [(66.1 \times 100)/14.5] = 9.254$ emu/g, whereas the experimental result showed a value of 8.9 emu/g. Similarly, the theoretical M_s of PAM–MC HGMNC was calculated as $M_s = [(66.1 \times 100)/9.7]$

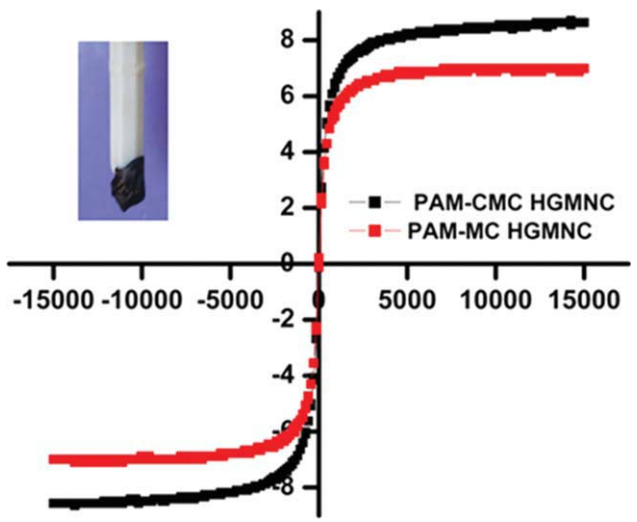

Figure 10 Magnetization saturation curves of the PAM–CMC HGMNCs and PAM–MC HGMNCs. [Color figure can be viewed in the online issue, which is available at wileyonlinelibrary.com.]

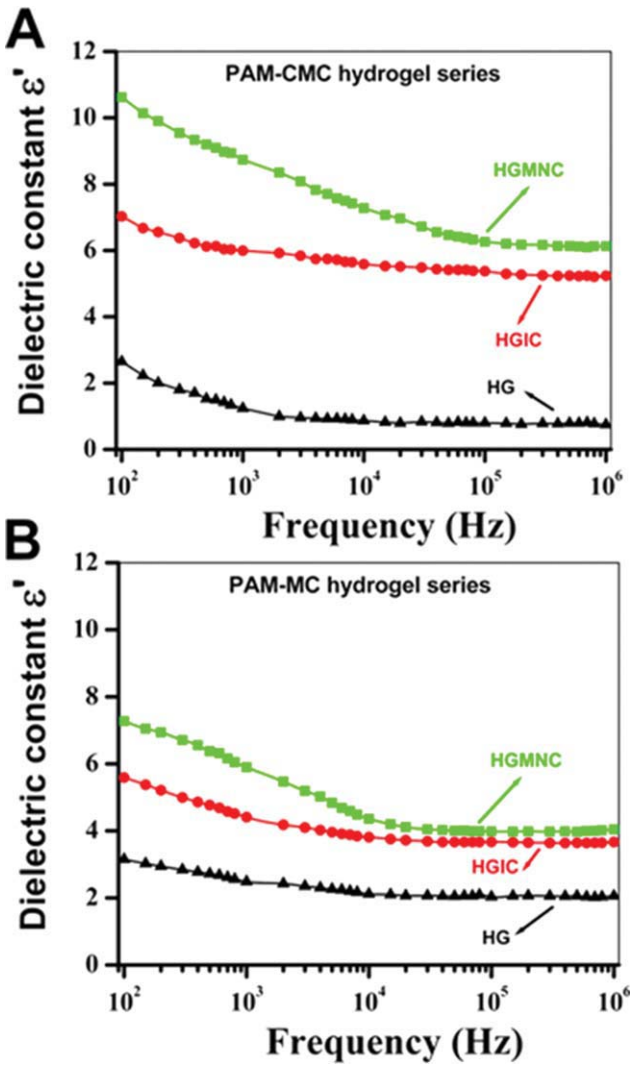

Figure 11 Dielectrical properties of HG, HGIC, and HGMNCs of (A) PAM–CMC and (B) PAM–MC hydrogels. [Color figure can be viewed in the online issue, which is available at wileyonlinelibrary.com.]

= 6.41 emu/g, and the experimental result was 6.4 emu/g. From these calculations, it could be inferred that the composites developed in this investigation contained a single domain of magnetic nanoparticles, within the hydrogel networks exhibiting a unique phenomenon of superparamagnetism.[36] According to the experimental results, the dried HGMNC (PAM–CMC HGMNC) was readily attracted to the poles of a free-standing magnet (inset of Fig. 10), indicating good magnetic properties.

Dielectrical measurements

Materials with high ε's are useful in the manufacturing of high-value capacitors/inductors and in recording media. In our investigation, an attempt was made to enhance the dielectrical constant of the hydrogels through the incorporation of Fe_3O_4 nanoparticles in the hydrogels. The dielectrical constants of the HGs and their HGICs and HGMNCs (HGMNCs) were measured in the frequency range of 10^2–10^6 Hz. From Figure 11, it was found that ε′ decreased with increasing frequency because of dielectric dispersion as a result of the lag of the molecules behind the alternation of the electric field at higher frequency.[37] Lower values of ε′ were recorded for the HGs. This could be explained by a great change in the structure of the gel due to crosslinking. This resulted in a spatial structure with a very high symmetry, as indicated previously, which decreased the polarizability of the molecules and, hence, ε′. Also, the formed spatial structures had enlarged side groups, and the molecules occupied more volume; this resulted in a decrease of the number of unit dipoles per unit volume, that is, ε′.[38] The iron ions in the hydrogels (HGICs) seemed to provide interchain spaces, which expanded with increasing temperature and showed no hindrance effect. This resulted in a high polarizability and, thereby, increased the ε′'s. The HGMNCs showed a further increase in the free volume with free spaces between the gel networks; this further improved their ε′'s. The overall ε′ order was noticed as HGMNC > HGIC > HG.

Curcumin loading and releasing studies

The loading efficiency of curcumin in the hydrogels was varied between the types of hydrogels. The order of efficiency was noticed as HGMNC (62%) > HG (51%) > HGIC (45%) for the PAM–CMC series and as HGMNC (66%) > HG (58%) > HGIC (51%) for the PAM–MC series. The higher loading in HGMNC was due to the presence of excess free space between the hydrogel networks because of nanoparticle formation and because the curcumin molecules were bound onto the surface of the nanoparticles. The lowest loading in HGIC may have been due to repulsive forces between iron salts and curcumin molecules, which, thereby, restricted the penetration of curcumin molecules into the hydrogel networks.

The aim of this study was to investigate curcumin delivery to various common diseases. *In vitro* curcumin release from the hydrogels was carried out in a pH 7.4 buffer solution at 37°C. The percentage cumulative release of curcumin from the hydrogel was calculated with eq. (2). The release profiles indicated that the HGMNCs showed higher releasing profiles than the HGs and HGICs [Fig. 12(A,B)]. Ionic attractions between the iron ions and drug resulted in the

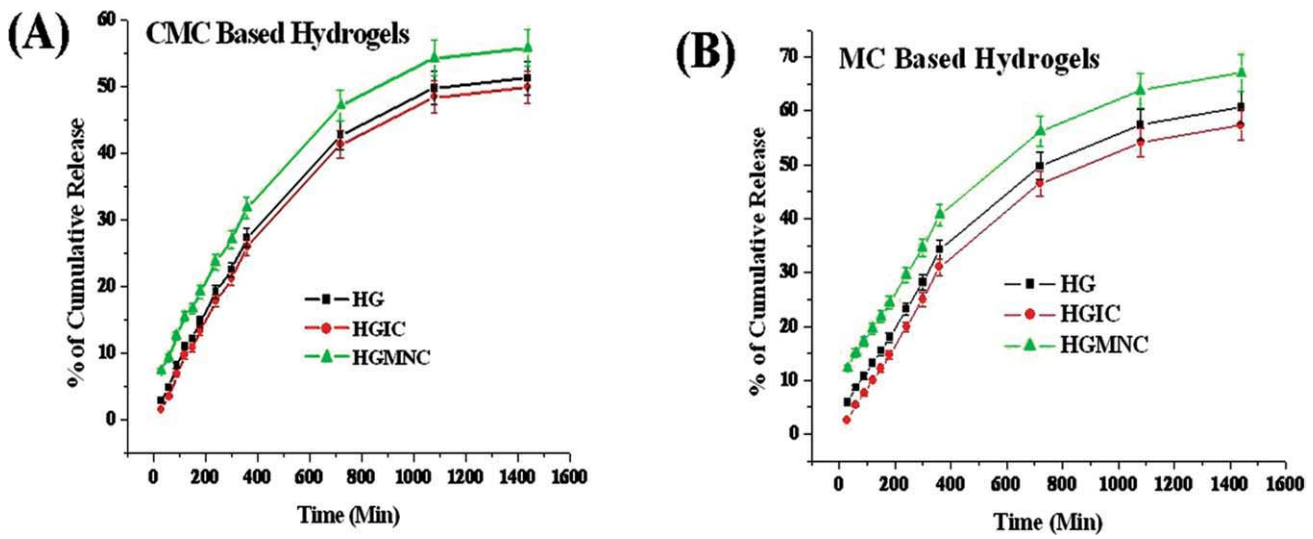

Figure 12 Curcumin release profiles of (A) CMC-based HG, HGIC, and HGMNCs and (B) MC-based HG, HGIC, and HGMNCs. [Color figure can be viewed in the online issue, which is available at wileyonlinelibrary.com.]

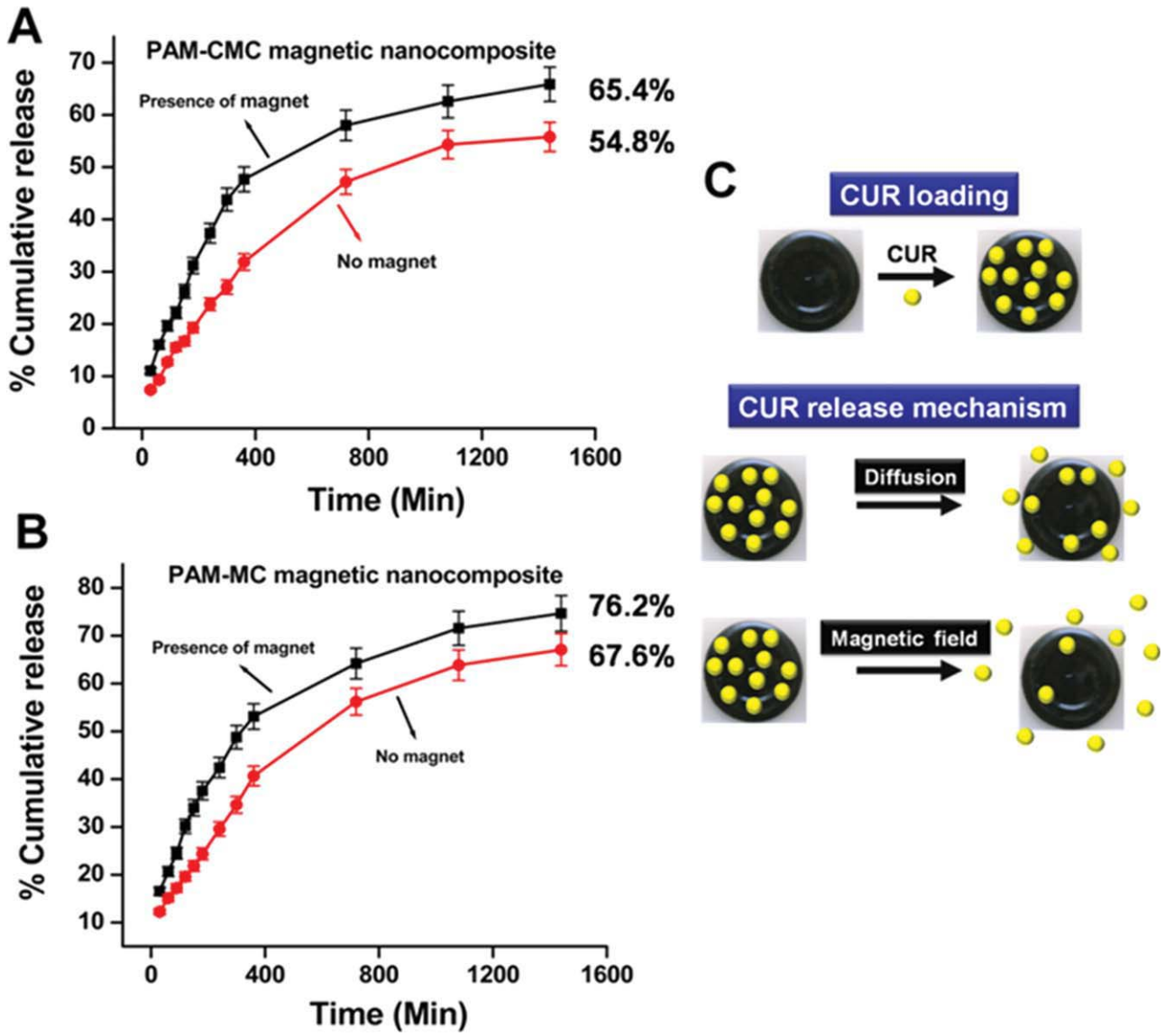

Figure 13 Curcumin (CUR) release profiles of HGMNCs of (A) PAM–CMC hydrogel, (B) PAM–MC hydrogel, and (C) curcumin loading and release schematic illustrations. [Color figure can be viewed in the online issue, which is available at wileyonlinelibrary.com.]

slower release of curcumin. The higher amount of curcumin release from HGMNCs was due to the presence of free space between the nanoparticles; this allowed drug molecules into the medium. The increase in the nanoparticle size resulted in increased drug loading and a larger fraction of drug molecules entrapped within the polymer matrix, with the result of a faster drug-release rate, dependent on both polymer breakdown and diffusion out of the matrix.

It is well known that the delivery of drugs from the hydrogel system can be controlled by external stimuli (in this case, an external magnetic field). The curcumin release from the HGMNCs was found to be in a sustained manner [Fig. 13(A,B), lower red curves]. This sustained behavior was obtained only

TABLE I
Percentage of Fe_3O_4, Encapsulation Efficiency, and Percentage Cumulative Release Data of HGMNCs

Type of hydrogel	$FeCl_2{\cdot}4H_2O$ (g)	$FeCl_3{\cdot}6H_2O$ (g)	Fe_3O_4 weight (%; TGA)	Curcumin drug loading (mg)	Encapsulation efficiency (%)	Cumulative release (without magnet; %)
PAM–CMC	2.1	5.8	14.5	3.12	62.4	54.8
PAM–MC	2.1	5.8	9.7	3.30	66.1	67.6

by the diffusion of curcumin into the external medium, which was PBS. Because of the hydrophobic nature of curcumin, a lower amount of drug was entrapped in the hydrogels. Therefore, these gels showed sustained drug-release profiles. However, the employment of an applied magnetic field with a magnet improved the delivery of curcumin from the HGMNCs into the medium [Fig. 13(A,B), upper black curves]. The experimental results showed a 10% increase in all of the stages of drug release, that is, at all time points. An improved release was caused by the alignment of magnetic nanoparticles by the external magnetic field; this, in turn, expands the hydrogel networks, which allowed a greater number of curcumin molecules to release into the medium. For this, a schematic illustration is presented in Figure 13(C). Table I describes the percentage of Fe_3O_4 formed in the HGMNCs, the encapsulation efficiency of curcumin, and the curcumin-releasing capacity of the HGMNCs.

CONCLUSIONS

HGMNCs based on PAM–CMC and PAM–MC were successfully developed. The formation of magnetic nanoparticles ($\sim$ 22 nm) in the hydrogel network was confirmed by SEM and TEM. The developed HGMNCs were characterized by FTIR spectroscopy, XRD, and thermal studies (TGA and DSC). Their inherent swelling properties were also investigated in detail. The magnetic properties of the developed HGMNCs were studied in detail. The incorporation of Fe_3O_4 nanoparticles in the hydrogels enhanced their dielectric properties so that the prepared hydrogel magnetic nanoparticles were used for the preparation of capacitors/inductors. The drug-releasing profiles of the hydrogel samples were also studied.

The authors thank Natural Remedies Private, Ltd., for the supply of curcumin.

References

1. Kamath, K. R.; Park, K. Adv Drug Delivery Rev 1993, 11, 59.
2. Hoffman, A. S. Adv Drug Delivery Rev 2002, 54, 3.
3. Dorkoosh, F. A.; Verhoefm, J. C.; Borchard, G.; Refiee-Tehrani, M.; Verheijden, J. H. M.; Junginger, H. E. Int J Pharm 2002, 247, 47.
4. Dorkoosh, F. A.; Herhoef, J. C.; Ambagts, M. H. C.; Tehrani, M. R.; Borchard, C.; Junginger, H. E. Eur J Pharm Sci 2002, 15, 433.
5. Achar, L.; Peppas, N. A. J Controlled Release 1994, 31, 271.
6. Zhuang, Y.; Chen, J.; Zhu, Z.; Yang, H. Polym Adv Technol 2000, 11, 192.
7. Liu, L.; Amit, C.; Feng, X. J Membr Sci 2008, 310, 66.
8. Kato, N.; Takizawa, Y.; Takahashi, F. J. J. Intell Mater Sys Struct 1997, 8, 588.
9. Panevo, D.; Stoilova, O.; Manolova, N.; Rashkov, I. E-Polymer 2004, 60, 1.
10. Adriane, K.; Huang, J.; Ding, D.; Chen, J.; Liu, Y. J Drug Target 2006, 14, 243.
11. Liang, Y. Y.; Zhang, L. M.; Jiang, W.; Li, W. Chem Phys Chem 2007, 8, 2367.
12. Kondo, A.; Fukuda, H. Ferment J Bioeng 1997, 84, 337.
13. Rao, L. L.; Ramanujan, R. V. J Mater Sci Mater Med 2004, 15, 1061.
14. Edelman, E. R.; Kost, J.; Bobeck, H.; Langer, R. J Biomed Mater Res 1985, 19, 67.
15. Kost, J.; Langer, R. Pharm Int 1986, 7, 60.
16. Edelman, E. R.; Brown, L.; Taylor, J.; Langer, R. J Biomed Mater Res 1987, 21, 339.
17. Satarkar, N. S.; Hilt, J. Z. J Controlled Release 2008, 130, 246.
18. Huang, L. Y.; Yang, M. C. J Mag Magn Mater 2007, 310, 2874.
19. Siegrist, T.; Vanderah, T. A. Eur J Inorg Chem 2003, 2003, 1483.
20. Buerkle, A.; Sarabandi, K. IEEE Trans Antennas Propag 2005, 53, 3436.
21. Bate, G. I.; Wohlfahrt, E. P. Ferromagnetic Materials; Amsterdam: North Holland, 1986; Vol. 2, p 381.
22. Wilson, J. L.; Poddar, P.; Frey, N. A.; Srikanth, H.; Mohomed, K.; Harmon, J. P.; Kotha, S.; Wachsmuth, J. J Appl Phys 2004, 95, 1439.
23. Chang, C.; Duan, B.; Cai, J.; Zhang, L. Eur Polym J 2010, 46, 92.
24. Herńndez, R.; Mijangos, C. Macromol Rapid Com 2009, 30, 176.
25. Sela, G. B.; Epelbaum, R.; Schaffer, M. Curr Med Chem 2010, 17, 190.
26. Jurenka, J. S. Altern Med Rev 2009, 14, 141.
27. Maheshwari, R. K.; Singh, A. K.; Gaddipati, J.; Srimal, R. C. Life Sci 2006, 78, 2081.
28. Strimpakos, A. S.; Sharma, R. A. Antioxid Redox Signal 2008, 10, 511.
29. Sharma, R. A.; Steward, W. P.; Gescher, A. J. Adv Exp Med Biol 2007, 595, 453.
30. Berlin, E.; Anderson, B. A.; Pallansch, M. J. J Dairy Sci 1973, 56, 685.
31. Murthy, P. S. K.; Mohan, Y. M.; Varaprasad, K.; Sreedhar, B.; Raju, K. M. J Colloid Interface 2008, 318, 217.
32. Sivudu, K. S.; Rhee, K. Y. Colloids Surf A 2009, 349, 29.
33. Vimala, K.; Sivudu, K. S.; Mohan, Y. M.; Sreedhar, B.; Raju, K. M. Carbohydr Polym 2009, 75, 463.
34. Huang, S. H.; Liao, M. H.; Chen, D. H. Biotechnol Prog 2003, 19, 1095.
35. Liu, S.; Zhang, L.; Zhou, J.; Xiang, J.; Sun, J.; Guan, J. Chem Mater 2008, 20, 3623.
36. Shinouda, H. G.; Hanna, A. A. J Appl Polym Sci 1977, 21, 1479.
37. El-Anwar, I. M.; Saad, M. Bull NRC Egypt 1983, 8, 151.
38. Anwar, I. M. E.; Nabawy, O. M. E.; Hennwii, S. A. E.; Salama, A. H. Chaos Solutions Fractals 2003, 11, 1303.